

pubs.acs.org/JCTC Article

Bacterial Analogs to Cholesterol Affect Dimerization of Proteorhodopsin and Modulates Preferred Dimer Interface

Eric Sefah and Blake Mertz*



Cite This: J. Chem. Theory Comput. 2021, 17, 2502-2512



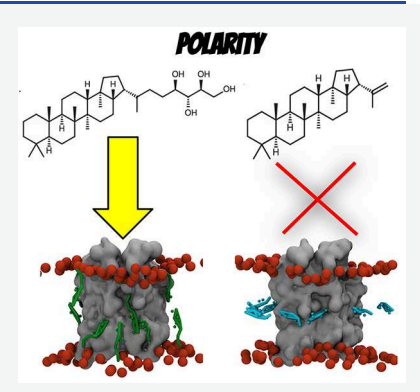
ACCESS

Metrics & More



Supporting Information

ABSTRACT: Hopanoids, the bacterial analogues of sterols, are ubiquitous in bacteria and play a significant role in organismal survival under stressful environments. Unlike sterols, hopanoids have a high degree of variation in the size and chemical nature of the substituent attached to the ring moiety, leading to different effects on the structure and dynamics of biological membranes. While it is understood that hopanoids can indirectly tune membrane physical properties, little is known on the role that hopanoids may play in affecting the organization and behavior of bacterial membrane proteins. In this work we used coarse-grained molecular dynamics simulations to characterize the effects of two hopanoids, diploptene (DPT) and bacteriohopanetetrol (BHT), on the oligomerization of proteorhodopsin (PR) in a model membrane composed of 1-palmitoyl-2-oleoyl-sn-glycero-3-phophoethanolamine (POPE) and 1-palmitoyl-2-oleoyl-sn-3-phosphoglycerol (POPG). PR is a bacterial membrane protein that functions as a light-activated proton pump. We chose PR based on its ability to adopt a distribution of oligomeric states in



different membrane environments. Furthermore, the efficiency of proton pumping in PR is intimately linked to its organization into oligomers. Our results reveal that both BHT and DPT indirectly affect dimerization by tuning membrane properties in a fashion that is concentration-dependent. Variation in their interaction with PR in the membrane-embedded and the cytoplasmic regions leads to distinctly different effects on the plasticity of the dimer interface. BHT has the ability to intercalate between monomers in the dimeric interface, whereas DPT shifts dimerization interactions via packing of the interleaflet region of the membrane. Our results show a direct relationship between hopanoid structure and lateral organization of PR, providing a first glimpse at how these bacterial analogues to eukaryotic sterols produce very similar biophysical effects within the cell membrane.

■ INTRODUCTION

G protein-coupled receptors (GPCRs) are the largest family of cell surface receptors in eukaryotes and are encoded by up to 4% of all human genes. It is therefore not surprising that they are the target for 30-40% of all drugs currently in use.2 An understanding of the mechanism of their signal transduction at the molecular level is pivotal to their more effective use as novel therapeutic agents.³ The canonical model for GPCR activation, based on a one ligand-one receptor interaction, ⁴⁻⁶ has been challenged by mounting evidence of receptor dimerization and/or formation of higher-order oligomers with functional cross-talk among protomers.7-10 Although it is widely accepted today that receptor dimerization potentially affects ontogeny, ligand-promoted regulation, pharmacology diversity, signal transduction, and internalization, 11 the notion still attracts skepticism because proximity-based assays (e.g., bioluminescence and fluorescence resonance energy transfer) do not provide information on direct protein-protein interactions. 8,12,13 In addition to the issue of stoichiometry with respect to GPCR activation, it has been suggested that membrane composition can tune interactions at receptor interfaces, thereby modulating oligomerization. In particular, multiple studies have revealed that cholesterol can influence the function, dynamics, and organization of receptors. 14,15

While the mechanism by which membrane cholesterol modulates GPCR dimerization is unclear, ¹⁴ several hypotheses have been proposed, including direct interactions that lead to conformational changes in the helical bundle ^{16,17} or indirectly by inducing changes in the membrane environment. ^{18,19}

Proteorhodopsin (PR) is a microbial membrane protein that acts as a light-driven proton pump. ^{20,21} PR is found in 13–80% of marine bacteria and archaea, ²² and it plays a potentially critical role in marine ecosystems. Expression of genes encoding for PR is directly involved in degradation of complex organic material as part of the carbon cycle, ^{23,24} and PR also provides a source of ATP during periods of nutrient deficiency. ²⁵ PR is an ideal model for studying oligomerization of heptahelical membrane proteins. It is predominantly found as a pentamer or hexamer in a membrane environment ^{26–29} yet can still function as a monomer. ²⁸ Oligomerization of PR

Received: November 10, 2020 Published: March 31, 2021





can be tuned both via membrane composition (e.g., detergents, bicelles, and bilayers^{27–29}) and by mutation of specific residues (W34^{29,30} and the E50/R51/D52 triad²⁷). In addition, oligomerization of PR affects the thermodynamics and kinetics of its photocycle,^{28,29} providing numerous ways in which to manipulate the environment of PR and observe the different behaviors of the protein.

One aspect of the connection between membrane environment and PR oligomerization that has been relatively unexplored is the role of hopanoids. Ten percent of bacteria possess genes to synthesize hopanoids, 31-33 comprising about 2-11 mol % of bacterial lipids in the inner and outer cell membrane. However, this percentage increases significantly in response to stressful conditions. Hopanoids are structurally similar to eukaryotic sterols (Figure 1A), with the ability to intercalate between membrane phospholipids and alter membrane fluidity. Despite their similarity, sterols and hopanoids alter membrane properties with different efficiencies. Similar to sterols and lipid rafts, there is evidence that hopanoids could support the formation of liquid-ordered phases, 42-44 but this is a subject of much debate.

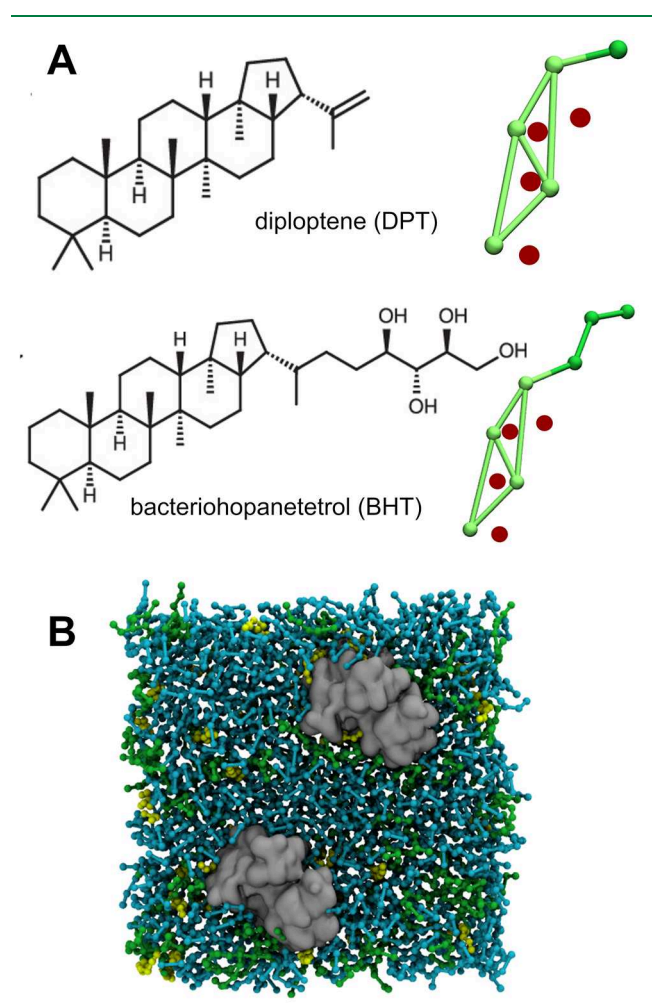


Figure 1. Hopanoids used in this study. (A) Chemical structure of DPT and BHT (left), with coarse-grained topology to represent hopanoids in MD simulations (right). Green balls and sticks represent CG beads, and red spheres are the virtual sites used in stabilizing their structures. (B) Snapshot of representative system of PR in POPE (cyan) and POPG (green) membrane in the presence of a hopanoid (yellow).

existence of such membrane microdomains in bacteria would have far-reaching effects on the kinetics of protein—protein and membrane-protein interactions and the thermodynamics of membrane fluctuations and remodeling.

Given the role of oligomerization on the function of PR and the prevalence of hopanoids in bacterial systems, we set out to characterize the effect that hopanoids have on lateral interactions between PR monomers in a membrane. Molecular dynamics (MD) simulations have been an invaluable tool in fundamental understanding of these types of interactions, both for sterol-protein interactions and protein—protein interactions. 52-54 In particular, coarse-grained MD simulations have been critical in providing these insights as they can access length and time scales that are relevant to membrane protein oligomerization. Few computational studies have been conducted on hopanoids; 55,56 this is the first to examine the effect of hopanoids on membrane proteins. In this study, we carried out coarse-grained MD simulations to determine the effect of two types of hopanoids, bacteriohopanetetrol (BHT) and diploptene (DPT), on the membrane environment and the ability of PR to form dimers, the first step in oligomerization. We discovered that BHT and DPT both lead to a condensing effect on the bilayer but in different manners. In addition, hopanoids decrease the propensity for PR dimerization through both short-range (high-affinity binding of BHT) and long-range (alteration of membrane biophysics) interactions.

METHODS

Coarse-Grained MD Simulation Setup. The structure of green proteorhodopsin (GPR) was obtained by generating a homology model using the X-ray crystal structure of blue proteorhodopsin (BPR) (PDB 4JQ6) as a template.³⁰ The retinal chromophore was removed from chain A, and missing loop regions were modeled into the structure using CHARMM.⁵⁷ Martinize.py⁵⁸ was used to convert the resulting structure into coarse-grained topology, employing the ElNeDyn model⁵⁹ with a force constant of 500 kJ/mol/nm² and a cutoff of 1.5 nm to constrain the secondary and tertiary structure of the protein. For monomeric systems, PR was aligned with its principal axis parallel to the z-axis, randomly rotated around the principal axis, and placed in a $7.5 \times 6.5 \times$ 11.5 nm box. For the dimeric systems, each monomer of PR was aligned with their respective principal axis parallel to the zaxis, randomly rotated around each respective principal axis, and placed at a minimum distance of 4 nm apart from one another in a $11 \times 11 \times 11$ nm box. For hopanoid-free systems, a lipid bilayer with a 3:1 ratio of POPE:POPG at a 120:1 (monomer) and 190:1 (dimer) lipid:protein ratio was used. For hopanoid-containing systems, BHT or DPT was added to the lipid mix at mole fractions of 0.1, 0.2, or 0.3. All PR-bilayer systems were constructed using insane.py. 60 Each system was solvated with polarizable MARTINI waters⁶¹ (3,000 for the monomer and 7,000 for the dimer) and NaCl ions added to neutralize the system and bring the concentration to 0.15 M. System sizes were approximately 11,000 particles for the monomer systems and 27,000 particles for the dimer systems. In addition to systems containing PR, we generated PR-free systems with a corresponding number of lipids, hopanoids, and waters, as a control.

The MARTINI force field version 2.2⁵⁸ was used for proteins, version 2.0⁶² for lipids, and specialized parameters using virtual sites for hopanoids.⁵⁶ Ten copies of each system were generated as described. The temperature was maintained

at 310 K using the velocity rescaling thermostat⁶³ with a coupling constant of $\tau_t = 1.0$ ps. The Parrinello-Rahman barostat⁶⁴ was used to control the pressure semi-isotropically at P = 1 bar with a coupling constant of $\tau_t = 12.0$ ps and compressibility of $3 \times 10^{-4} \text{ bar}^{-1}$. The Verlet scheme with a straight LJ cutoff at 1.1 nm and reaction-field electrostatics with a Coulomb cutoff at 1.1 nm were employed. All production simulations were run with GROMACS 2016.665 using a 15 fs time step. Fifteen femtoseconds was chosen for stability of the protein-lipid-hopanoid mix. Simulation lengths varied from 10 to 20 µs for monomer systems and slightly longer for dimer systems. Decorrelation times (τ_{decorr}) were calculated for each set of simulations,66 in order to determine the time scales for sufficient mixing of hopanoids (Figure S1). For each set, at least 7 μ s of trajectory beyond the decorrelation time was collected and used for the analyses (Tables 1 and 2).

Table 1. List of Monomeric PR Systems Simulated in This Work

| hopanoid | mol % | time/ μ s | trajectories | total/ μ s |
|----------|-------|---------------|--------------|----------------|
| none | 0% | 10 | 10 | 100 |
| BHT | 10% | 18 | 10 | 180 |
| | 20% | 18 | 10 | 180 |
| | 30% | 18 | 10 | 180 |
| DPT | 10% | 10 | 10 | 100 |
| | 20% | 10 | 10 | 100 |
| | 30% | 18 | 10 | 180 |

Table 2. List of Dimeric PR Systems Simulated in This Work

| hopanoid | mol % | time/ μ s | trajectories | total/ μ s |
|----------|-------|---------------|--------------|----------------|
| none | 0% | 10 | 5 | 50 |
| BHT | 10% | 18 | 5 | 90 |
| | 20% | 20 | 5 | 100 |
| | 30% | 20 | 5 | 100 |
| DPT | 10% | 12 | 5 | 60 |
| | 20% | 12 | 5 | 60 |
| | 30% | 12 | 5 | 60 |

Docking. We performed blind docking of hopanoids to the atomistic homology model of GPR mentioned above using AutoDock Vina. The protein structure was prepared by adding polar hydrogens in AutoDock Tools. The search space was restricted to the transmembrane region of PR with a $40 \times 40 \times 42$ Å box in the x, y, and z dimensions, respectively. An exhaustiveness parameter of 200 was used, with all other Vina settings at default values. Binding modes were visualized in PyMOL.

Analysis. Membrane area and bilayer thickness were calculated using the Fast Analysis Toolbox for Simulations of Lipid Membranes (FATSLiM).⁶⁹ Phosphate beads were chosen as the headgroup for each of POPE and POPG in the analysis. Order parameters were calculated using the Lightweight Object-Oriented Structure library (LOOS).⁷⁰ Because CG beads lack hydrogens, the entire lipid molecule was used to calculate the order parameter. LOOS finds the principal axis of the selection and calculates the angle it makes with the second and third axes. LOOS was also used to calculate cylindrical thickness of the membrane, defined as the average thickness of the membrane as a function of the lateral

distance from the center of mass of the protein. The tilt angle of lipids was obtained by computing the angle between the vector defined by the first bead on the ring moiety (R1), either the last bead representing the hydrocarbon attachment of DPT (C1) or BHT (C3), and the positive z axis using GROMACS tools. Protein-hopanoid interactions were calculated using PyLipID,⁵¹ a python library for the analysis of protein-lipid interactions. In PyLipID, protein-lipid contact frequencies are determined using a minimum distance cutoff. A correlationbased community detection is then used to assign regions of high-lipid interaction using protein residues as nodes and the interaction frequency between a pair of residues and molecules of a particular lipid type as edges. Interaction durations are also estimated from a dual cutoff scheme in which an interaction begins when the lipid molecule enters the minimum cutoff and ends when it exits the maximum cutoff. A dissociation constant (k_{off}) is then calculated for each residue and each interaction site using the normalized survival function in eq 1, where N_i is the number of continuous appearances occurring in the simulation, *T* is the total simulation time, and $n_i(\nu_i\nu_i + \Delta t) = 1$ if a contact continued for a duration of Δt after its formation at time $\nu = 0$ or $n_i(\nu, \nu + \Delta t) = 0$ if otherwise. The survival function was fitted to the biexponential in eq 2. The smaller kwas taken as the $k_{\rm off}$ and residence time was calculated as the inverse of koff values. Details of PyLipID and it is implementation, including tutorials, can be found at (https://github.com/wlsong/PyLipID). We chose 0.5 and 0.7 nm for our minimum and maximum cutoff, respectively, based on the rdf of the first lipid shell (Figure S2). Dimer interfaces were identified from both cluster analysis and inhouse scripts. The gromos clustering algorithm⁷¹ implemented in GROMACS was used, with an rmsd cutoff of 1.5 nm. Protomers were considered to be interacting with each other when the minimum distance between them was less than 0.7

$$\sigma(t) = \frac{1}{N_j} \frac{1}{T - \Delta t} \sum_{j=1}^{N_j} \sum_{\nu=0}^{T} n_j(\nu, \nu + \Delta t)$$
 (1)

$$y = Ae^{-k_1\Delta t} + Be^{-k_2\Delta t} \tag{2}$$

■ RESULTS AND DISCUSSION

Hopanoids Exert Different Effects on the Bilayer Environment. Since previous MD studies had shown that the presence of hopanoids have a condensing effect on bilayer systems, ^{55,56} our first step was to determine if hopanoids had a similar effect on the bilayer environment in the presence of PR. Addition of 10 mol % BHT or DPT led to a condensing effect on the lateral plane of the bilayer, with a decrease in area per lipid of POPE of > 0.15 nm² compared to the hopanoid-free system (Figure 2A). As the mole fraction of hopanoids was increased to 20% and 30%, respectively, we observed a nonlinear decrease in the area per lipid. Interestingly, DPT had a larger effect on the decrease in area per lipid compared to BHT (almost 0.05 nm²). For all bilayer-based analysis, results were consistent across lipid-only, monomeric, and dimeric PR systems.

In order to compensate for the decrease in area per lipid, the thickness along the bilayer normal will increase. We observed a linear trend with an increase in mole fraction of hopanoids, with a greater increase occurring in the DPT-containing systems (Figure 2B). Despite the similar effects that BHT and

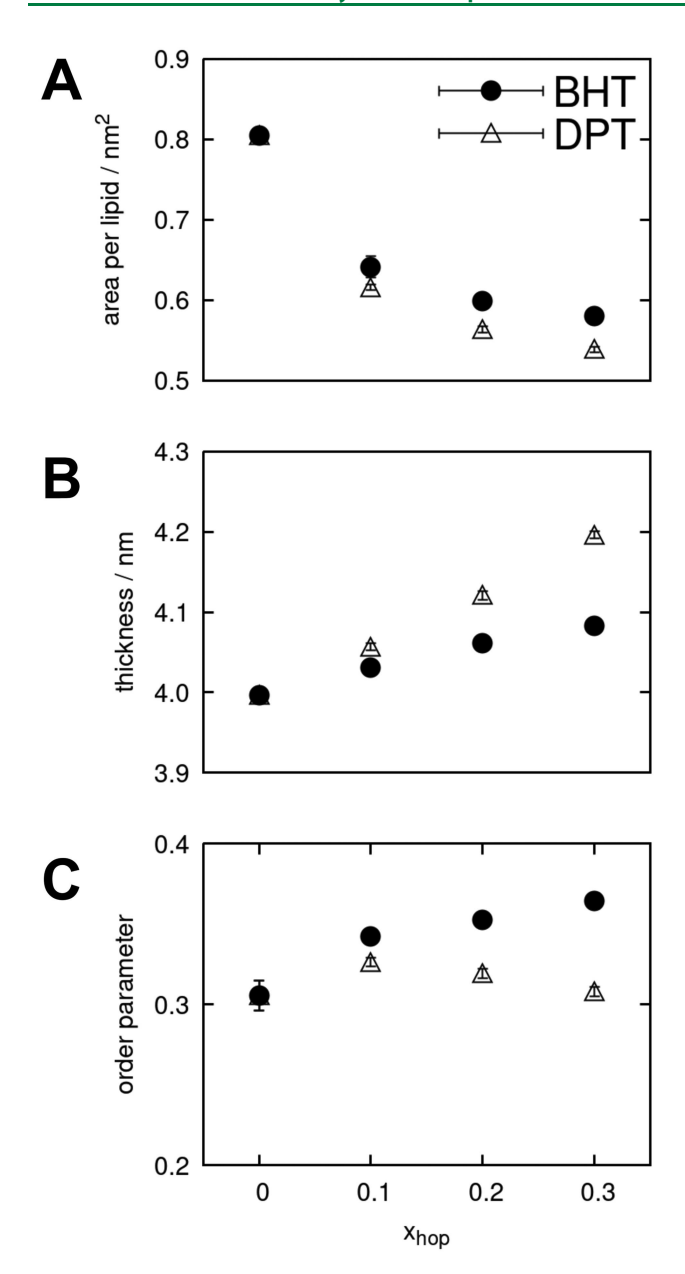


Figure 2. Hopanoids increase phospholipid packing density in different ways. (A) Area per lipid of POPE containing 0 to 30 mol % of hopanoid. (B) Membrane thickness as a function of mol % of hopanoids. (C) Molecular order parameter of POPE as a function of mol % of hopanoids.

DPT have on the dimensions of the bilayer, it appears that they accomplish this in different ways. For BHT, the bilayer becomes more ordered, but with DPT, the bilayer becomes progressively more disordered (Figure 2C). Each of these trends was also observed for POPG (Figure S3). This behavior of the bilayer indicates that different physicochemical properties of hopanoids could contribute to localized areas of order or disorder within the membrane, much like cholesterol does in ordering the plasma membrane of eukaryotes. ⁴⁷

Orientation of Hopanoids Is Correlated with Preferential Interaction with PR. Seeing that BHT and DPT had opposite effects on the ordering of the lipid bilayer, we wanted to determine the extent to which this discrepancy was a localized effect. In hopanoid-free systems, we observe a noticeable increase in the bilayer thickness within 8 Å in the

xy-plane of the surface of PR, suggesting there is some degree of hydrophobic mismatch with the POPE and POPG lipids (Figure 3A). Upon addition of hopanoids, BHT and DPT have different degrees of influence on the bilayer with respect to PR. For BHT, there is no increase in thickness proximal to PR and a very slight increase in thickness in the distal portions of the bilayer. At 10 mol % DPT, there is no increase in bilayer thickness near PR, but ~1 Å increase in thickness in the rest of the bilayer. At 20 and 30 mol %, an increase in bilayer thickness still occurs, with the increase taking place in all areas of the membrane (Figure 3A, right). This would suggest that either there is enough space and conformational flexibility in the bilayer near PR to accommodate the presence of 10% DPT or that DPT does not effectively bind to the bilayer-exposed surface of PR.

The answer to this difference in behavior lies in the organization of hopanoids in the membrane. Much like previous protein-free studies, 55,56 the orientation of BHT is nearly parallel with the membrane normal ($\sim 20^{\circ}$, Figure 3B,C, left). The extensive hydroxylated aliphatic chain leads to favorable polar interactions with the zwitterionic and anionic PE and PG headgroups in the phospholipids of the bilayer, allowing BHT to intercalate between the lipids, increasing the ordering of the acyl chains, having a lesser effect on increase in bilayer thickness, and significantly increasing decorrelation times. This behavior is very similar to cholesterol, in that the triterpenoid rings induce ordering of the acyl chains in the hydrophobic interior while the polar hydroxyl groups reside in the headgroup region, 72,73 ultimately leading to a decrease in area per lipid as a function of cholesterol concentration. Unlike BHT, DPT lacks the extended polar group to stabilize interactions that anchor the hopanoid in the headgroup region and instead adopts orientations that are roughly parallel to the lateral plane of the bilayer (i.e., ranging from tilted (45°) to completely orthogonal (90°) to the membrane normal). This leads to DPT being localized to the interleaflet region in the bilayer, creating a "sandwich" effect whereby an increase in mole fraction of DPT directly increases bilayer thickness (Figure 3B,C, right).

A closer look at the molecular interactions between PR and the hopanoids reveals that the orientation of BHT makes it possible for the hopanoid to have high-affinity interactions with the membrane protein. This is not surprising, as several classes of eukaryotic membrane proteins possess cholesterol or hopanoid binding sites that are relevant to function or organization within the membrane, 49,74,75 often referred to as the cholesterol consensus motif (CCM)⁷⁶ or the cholesterol recognition/interaction amino acid consensus sequence (CRAC domain). 77,78 From the calculated residence times a stark contrast exists in the ability of BHT and DPT to interact with PR. At concentrations as low as 10 mol % of BHT, we observe two distinct interaction sites with PR, corresponding to TM helices A/B/C and F/G, each with residence times of 7.0 µs (Table S1 and Figure 4). Furthermore, both sites involve strong interactions with one and three phenylalanine residues, respectively, hinting at the possibility of a π -stacking interaction with BHT rings. The same interactions are identified in the 20 and 30 mol % BHT systems as well, along with two others in each system. Interestingly, the interaction site that maps to helices F/G (residues $I^{232}LFGL^{236})$ overlaps with \bar{a} putative CARC motif (a reverse CRAC motif). The presence of CRAC motifs in bacterial membrane proteins is largely unexplored but is not completely

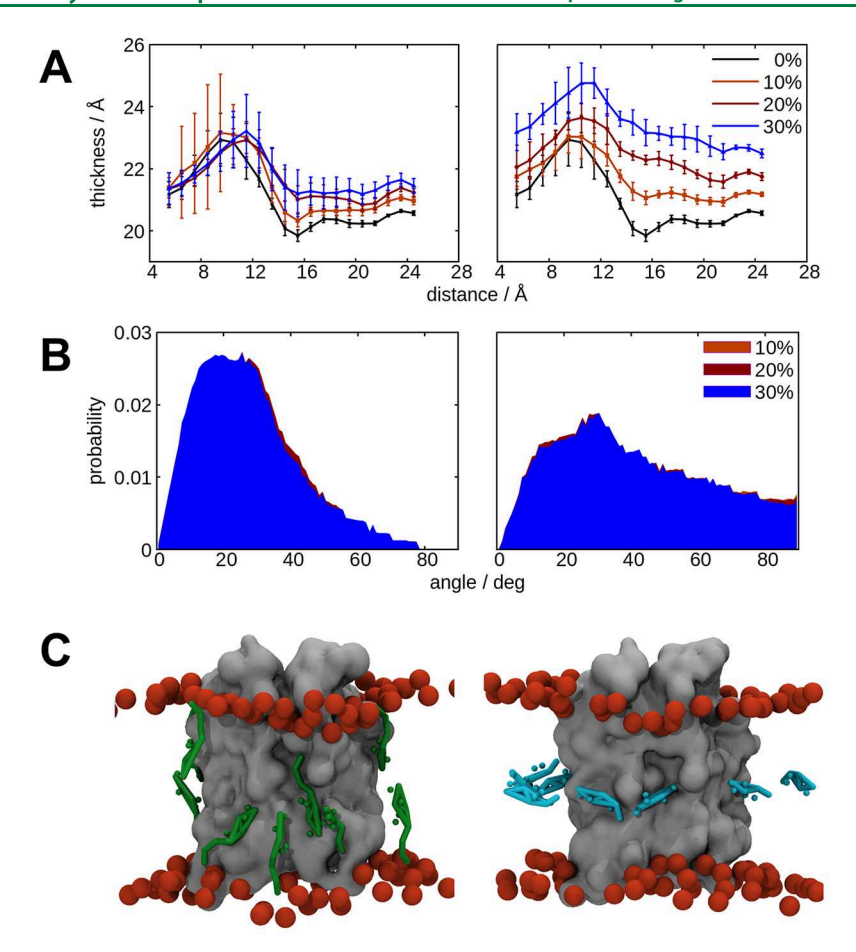


Figure 3. Hopanoid orientation tunes increase in bilayer thickness proximal to PR. (A) Average thickness of the bilayer as a function of distance from the center of mass of PR. Left: BHT-containing systems. Right: DPT-containing systems. (B) Probability distribution of the tilt angle of hopanoids with respect to the membrane normal. Left: BHT; right: DPT. (C) Representative snapshots showing orientation of BHT (left) and DPT (right), respectively.

surprising, as microbial rhodopsins like PR share the same 7TM topology as GPCRs. In contrast, for DPT we observe nonspecific interactions with PR: any interactions with the corresponding sites are transient (nearly all < 100 ns). This is consistent with our analysis above, as the orientation of DPT is orthogonal to the principal axes of PR in the membrane. At higher concentrations of hopanoids, these preferential interaction sites persist with a slight increase in residence times.

Blind docking of BHT or DPT to PR agrees well with our MD results and provides additional context to the nature of these hopanoid-protein interactions. In general, both hopanoids form complexes with PR that are parallel to the principal axis of the protein, with DPT (-7.4 kcal/mol) binding slightly better than BHT (-6.7 kcal/mol). However, the locations of binding are markedly different: BHT docks to the interaction site on helices F/G, similar to our MD simulations, whereas DPT docks to multiple areas (most frequently between helices A/G). In all poses where complexes form between helices F/G, F234 is critical to stabilizing binding, indicating that π – π stacking interactions play a role in PR-hopanoid interactions. Although the docking shows that both BHT and DPT have shape-based complementarity with the surface of PR, it is clear from our MD simulations that DPT interactions with PR are more transient, most likely because of their preferred orientation parallel to the midplane of the bilayer.

BHT interacts more effectively with monomeric PR than DPT for two reasons: (1) productive hopanoid-PR complexes form more frequently with BHT (most likely due to its orientation within the bilayer) and (2) association takes place on a significantly longer time scale. We have already established that BHT orients parallel to the membrane normal, allowing the planar face of the triterpenoid ring to interact with the hydrophobic surface of PR in the interior of the bilayer, while at the same time, the polar head interacts favorably with the lipid headgroups, much like cholesterol. This correlates to a markedly larger number of amino acid residues for BHT to interact with, as seen in the residence times (Figure 4 and Table S1). Not only does this orientation provide more opportunities for a bound complex to form, it maximizes the surface area available to utilize van der Waals forces to stabilize interactions between BHT and PR.

Little change occurs in the number and size of interactions between either BHT or DPT and PR (Figure S4), indicating that even at 10 mol % hopanoids all possible interaction sites have been sampled. The most distinguishing characteristics between the two types of interactions are that BHT has a slightly higher number of interactions with surface area > 10 nm². However, we do observe an increase in the residence time of bound hopanoids as their respective concentrations increase (Figure 5 and Table S1). This suggests a direct relationship between the strength of interactions and hopanoid concen-

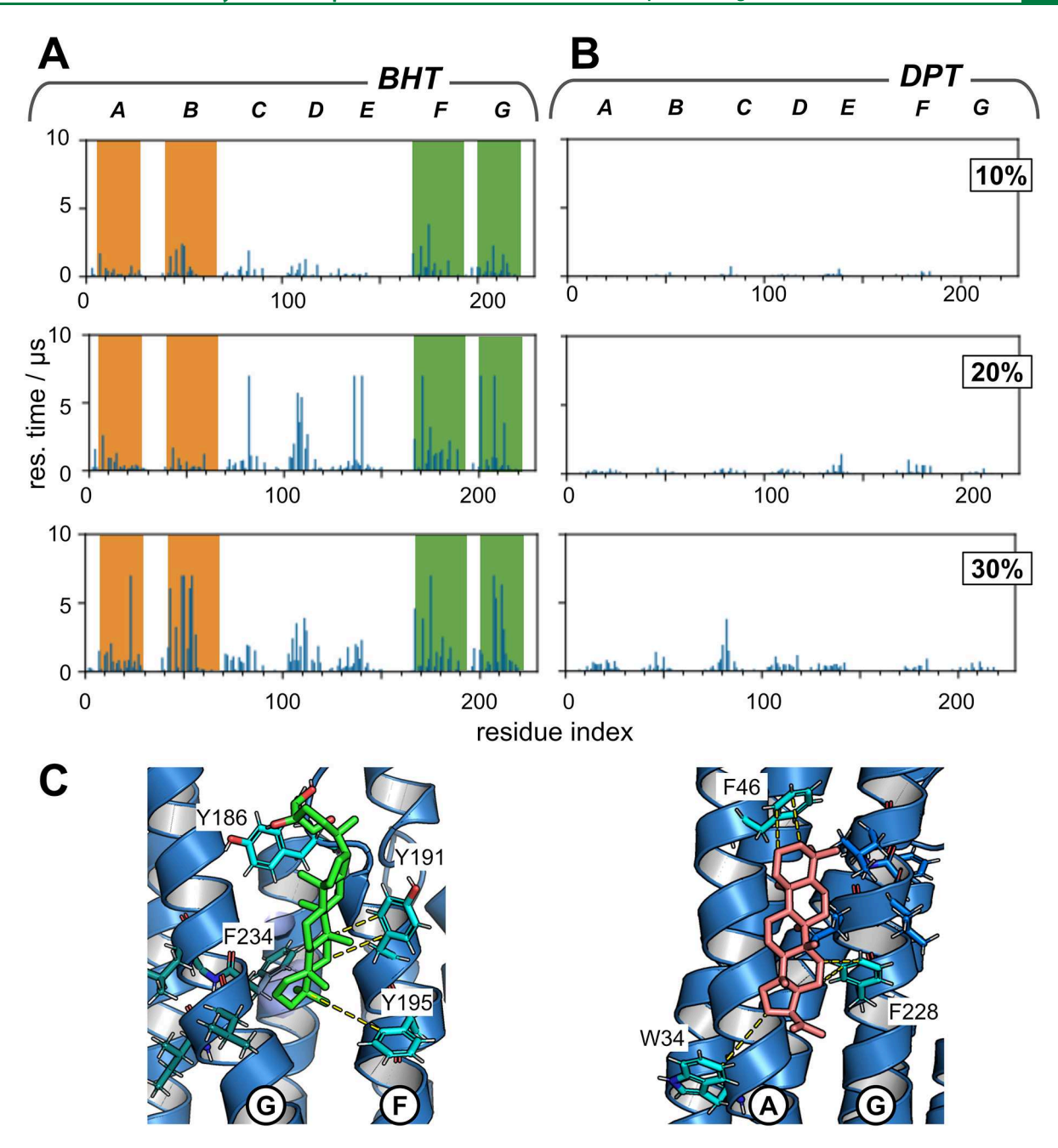


Figure 4. BHT binds to PR significantly longer than DPT. (A) Residence times for 10, 20, and 30 mol % BHT. Residence time is defined as the average length of a continuous interaction of hopanoids with a given residue. (B) Residence times at 10, 20, and 30 mol % DPT. (C) Snapshots of the lowest-energy binding poses for BHT (left) and DPT (right) to PR.

tration. For BHT, this implies that higher concentrations will more likely exclude possible interactions of residues at the protein surface with other membrane components or proteins, the latter of which directly affects dimerization of PR, as will be discussed below. For DPT, this effect is not as pronounced, since the residence times largely remain below 1 μ s even at 30 mol % DPT.

Hopanoids Interfere with Oligomerization of PR. Upon determining that several hopanoid interaction sites were present on PR, we wanted to determine the ability for BHT and DPT to enhance or reduce the likelihood of dimerization in PR. PR has been used as a model system to characterize the relationship between membrane environment and oligomerization, ^{27,80,81} and it has also been shown that oligomerization of

PR is directly related to the efficiency and kinetics of proton pumping. ^{28,29,82} It is common for other microbial rhodopsins to organize into higher-order oligomeric states, such as bacteriorhodopsin, ⁸³ the sodium pump KR2, ⁸⁴ and the Gloebacter rhodopsin proton pump. ⁸⁵ However, to this date, PR is the only protein whose function is known to be directly affected by oligomerization.

We conducted simulations with the same series of mole fractions of hopanoids, this time with two monomers of PR in a lipid bilayer that were allowed to freely associate and dissociate. In the lipid-only system, helices A and E were predominantly involved in dimeric interactions, with multiple interfaces available for dimerization (Figure 6A). The observed dimeric interface is different from the pentameric and

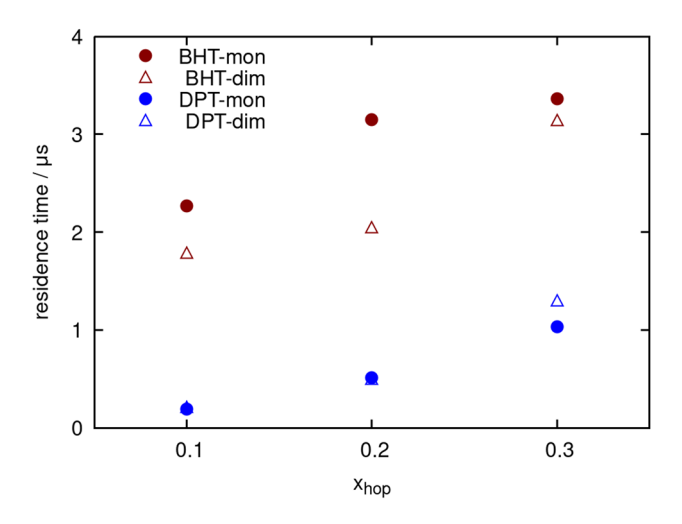


Figure 5. Residence times increase as a function of hopanoid concentration and with respect to BHT or DPT. Average lipid interaction site residence times calculated from averaging all residence times from the normalized survival functions using eqs 1 and 2.

hexameric arrangements in the X-ray crystal structure of blue PR,³⁰ where the protomer-protomer interface is formed between helices A and B and helices G and C (Figure 6A, inset). This would indicate that there are multiple interfaces that can form during assembly of higher-order oligomers and that the final arrangement of protomers occurs only after overcoming the energy barriers potentially associated with rearrangement from nonoligomeric interfaces. Upon addition of hopanoids, a marked shift in dimerization is observed. With 10 mol % BHT, interaction between the A and E interfaces and in the overall number of interfaces significantly decrease, with a slight increase in the interaction between helix F of the first monomer and helix A of the second monomer (Figure 6B, left). As the amount of BHT increases to 20 and 30 mol %, the majority of dimerization interactions are abolished (Figure 6C,D, left). Likewise, in 10 mol % DPT, most interfaces disappear, the only notable exception being an interface between helices A and B on the first monomer and helices D-F on the second monomer (Figure 6B, right). However, in a 20 and 30 mol % DPT system, that dimerization interface undergoes a major shift toward a symmetric interaction between helices A and B on both monomers (Figure 6C,D, right), consistent with the pentameric and hexameric forms of PR.

Moving down to the level of hopanoid-PR interactions reveals similar behavior. As with the monomeric systems, a large discrepancy exists in residence times between BHT (multi-µs) and DPT (hundreds of ns) (Table S2). As hopanoid concentration increases, we observe a gradual increase in residence time (Figure 5). In addition, the number and size of these interaction sites remain similar to what we observed for the monomeric systems (Figure S5). However, the location of these interaction sites and the nature of these interactions have a marked shift from the monomeric systems that are consistent with our identification of TM helix-helix interactions described above. For the BHT systems, the most predominant interaction sites are now among helices B, C, and D (Figure S6A), which coincide with the helices that are not involved with protein-protein interactions. For DPT, interactions with PR are still transient at 10 and 20 mol %; at 30 mol %, DPT forms interactions that last 500 ns up to 3 μ s

but are localized to the F/G and A/B helical interfaces (Figure S6B). It would appear that DPT either has little effect on monomer–monomer interactions in PR or can contribute to the stabilization of the dimeric interface. (Exact determination of that effect is the subject of future studies.) Our blind docking results suggest that stable complexes between hopanoids and PR are driven in large part by $\pi-\pi$ stacking interactions, regardless of the exact location on the surface of PR, and that hydrogen-bonding interactions between the hydroxyl groups of BHT and polar residues in PR can also aid in complex formation (Figure 4). These results in combination with the MD data provide an indication to how BHT and DPT influence PR–PR interactions in subtle yet different ways.

So what do our results tell us about the role of hopanoids and the process of oligomerization of PR? First, even though BHT and DPT possess the same triterpenoid scaffold, they can have very different biophysical effects on the membrane. In some ways, they are similar to cholesterol, in the fact that they condense the bilayer and slow down lateral diffusion of proteins. (It is possible that these hopanoids could contribute to formation of raft-like domains, but that is outside the scope of this study.) Spontaneous formation of higher-order oligomers of PR can follow many different pathways. On the basis of our results, there are multiple configurations that can form transiently stable dimers. Progression to higher-order oligomers (e.g., pentamers and hexamers) would require dissociation of asymmetric dimers to allow for rotation around the principle axis of each respective protein and formation of more stable dimers. In addition, PR needs to be present in high enough concentrations to facilitate formation of higher-order oligomers; our simulations were designed to focus on dimer formation with a lipid:protein ratio of 100:1, which is much higher than what is typically found in bacteria. Hopanoids may play a cooperative or inhibitory role in the process of oligomerization. For example, BHT may bind to surfaces of PR (like on helix A) that prevent formation of stable protomerprotomer interfaces. Conversely, DPT at 20 mol % favors the interaction between helices A and B of neighboring protomers that is critical to the pentamer and heaxmer X-ray crystal structures. It is well-established that hopanoids play an important biological role in bacteria, and our results make a case that this effect is rooted in the biophysical interactions they have with both the lipid bilayer and integral membrane proteins.

While the MARTINI model has the immense advantage of providing speedups in MD simulations an order of magnitude greater than atomistic simulations, it must also be applied carefully to membrane systems. This is particularly important with respect to membrane phenomena associated with lateral interactions within the bilayer (i.e., binding), as MARTINI 2.2 under-compensates for free energy barriers between integral membrane proteins, which can lead to enhanced association. 86-88 Several potential solutions exist to address this issue, each with advantages and disadvantages. Removal of the elastic network applied to retain protein structure allows for greater fluctuation of the heptahelical bundle and identification of novel interaction sites for cholesterol binding and dimerization⁸⁶ but remains relatively untested. Reparameterization of the MARTINI force field could be carried out to correct for these deficiencies⁸⁷ but requires rigorous testing and is currently being implemented in MARTINI 3.0. The most common corrective means has been to massively sample each respective system (hundreds of μ s to ms in aggregate

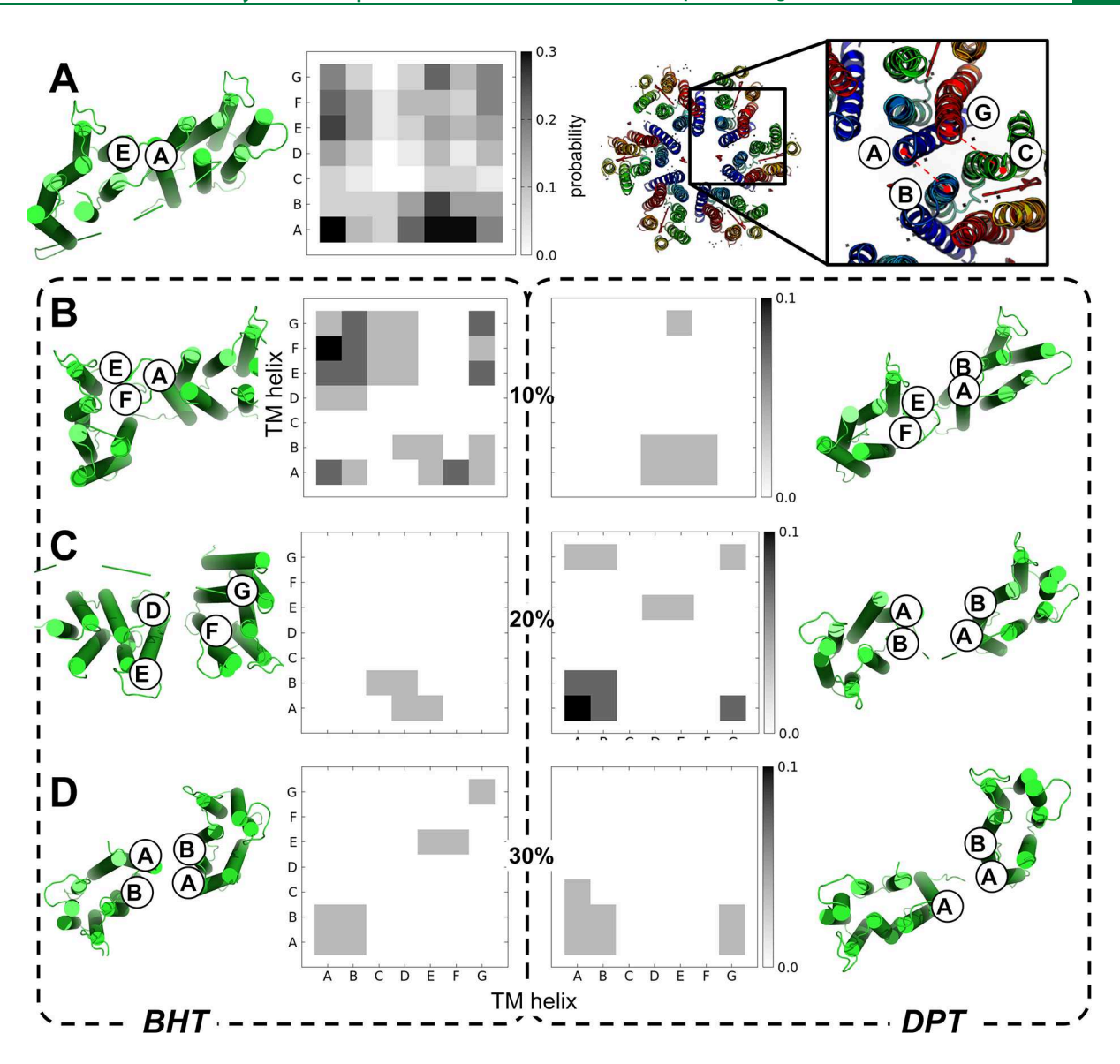


Figure 6. Hopanoids alter the dimerization interface of PR. (A) Left: probability matrix for helix—helix interaction between two PR monomers in a POPE:POPG lipid bilayer. A snapshot of the most likely dimeric interface is shown in green cylinders. Right: crystal structure of the hexamer of BPR (PDB 4JQ6), with inset showing the symmetric monomer—monomer interface. Interaction is defined as less than 0.7 nm. Right: (B) probability for helix—helix interaction between PR monomers in POPE:POPG bilayer with 10% BHT (left) or DPT (right). (C) Probability for helix—helix interaction between PR monomers in POPE:POPG bilayer with 20% BHT (left) or DPT (right). (D) Probability for helix—helix interaction between PR monomers in POPE:POPG bilayer with 30% BHT (left) or DPT (right).

simulation time), in order to allow for a rigorous statistical analysis of system characteristics that can compensate for an imperfect model. ^{51,52,89,90} This is the particular approach taken here, and we have done our best to account for these effects, both in our system setup and analysis of the results.

CONCLUSIONS

We have shown that both BHT and DPT induce changes in bilayer properties which are concentration dependent and also reflect the chemical nature of the hopanoid. While BHT shows no variability in membrane properties in regions around the protein, it appears DPT is capable of inducing variations in the lateral membrane dimensions that are concentration-dependent. We find that this has a consequence for dimerization at higher concentrations, especially in DPT-containing systems. While at lower concentrations both hopanoids compensate for

hydrophobic mismatch between the protein's hydrophobic stretch and membrane hydrophobic thickness, this is over-compensated for at higher concentrations of DPT, resulting in a steep decline in dimerization. A saturation of both hopanoids within the membrane beyond a certain point prevents dimerization altogether.

We have also shown that the orientation of BHT in the membrane, parallel to the principal axis of the protein, enhances interaction with the protein, both within the transmembrane domain as well as with residues in the receptor loop regions, resulting in more high-quality occupancy sites compared to DPT. These high-quality occupancy sites compete with potential dimer interfaces, resulting in a decrease in plasticity of the interfaces and abolishing some altogether. Our results show a direct and indirect modulation of receptor dimerization by hopanoids that could prove to be useful in the

design of receptors with desirable functionalities for both therapeutic and alternative energy applications.

ASSOCIATED CONTENT

50 Supporting Information

The Supporting Information is available free of charge at https://pubs.acs.org/doi/10.1021/acs.jctc.0c01174.

Further analyses revealing effect of hopanoids on membrane lipids and subsequent modulation of dimerization interface (PDF)

AUTHOR INFORMATION

Corresponding Author

Blake Mertz – C. Eugene Bennett Department of Chemistry and WVU Cancer Institute, West Virginia University, Morgantown, West Virginia 26506, United States;
orcid.org/0000-0002-7677-0496; Email: blake.mertz@mail.wvu.edu

Author

Eric Sefah — C. Eugene Bennett Department of Chemistry, West Virginia University, Morgantown, West Virginia 26506, United States

Complete contact information is available at: https://pubs.acs.org/10.1021/acs.jctc.0c01174

Notes

The authors declare no competing financial interest.

■ ACKNOWLEDGMENTS

The authors thank members of the Mertz lab for useful feedback, and the authors would like to specifically thank Ben Wylie for the inspiration to undertake this project. This work was supported by the NSF MCB-1714888 (E.S., B.M.). Computational time was provided through WVU Research Computing and XSEDE allocation no. TG-MCB130040.

REFERENCES

- (1) Matthews, J. M.; Sunde, M. Dimers, oligomers, everywhere. Protein Dimerization and Oligomerization in Biology 2012, 747, 1–18.
- (2) Hauser, A. S.; Attwood, M. M.; Rask-Andersen, M.; Schiöth, H. B.; Gloriam, D. E. Trends in GPCR drug discovery: new agents, targets and indications. *Nat. Rev. Drug Discovery* **2017**, *16*, 829–842.
- (3) Rossi, M.; Maggio, R.; Fasciani, I.; Scarselli, M. G-Protein-Coupled Receptor Dimers; Springer, 2017; pp 3–14.
- (4) Kuszak, A. J.; Pitchiaya, S.; Anand, J. P.; Mosberg, H. I.; Walter, N. G.; Sunahara, R. K. Purification and Functional Reconstitution of Monomeric μ -Opioid Receptors Allosteric Modulation of Agonist Binding by Gi2. *J. Biol. Chem.* **2009**, 284, 26732–26741.
- (5) Whorton, M. R.; Jastrzebska, B.; Park, P. S.-H.; Fotiadis, D.; Engel, A.; Palczewski, K.; Sunahara, R. K. Efficient coupling of transducin to monomeric rhodopsin in a phospholipid bilayer. *J. Biol. Chem.* **2008**, 283, 4387–4394.
- (6) Whorton, M. R.; Bokoch, M. P.; Rasmussen, S. G.; Huang, B.; Zare, R. N.; Kobilka, B.; Sunahara, R. K. A monomeric G protein-coupled receptor isolated in a high-density lipoprotein particle efficiently activates its G protein. *Proc. Natl. Acad. Sci. U. S. A.* **2007**, *104*, 7682–7687.
- (7) Marshall, F. H.; Jones, K. A.; Kaupmann, K.; Bettler, B. GABAB receptors-the first 7TM heterodimers. *Trends Pharmacol. Sci.* **1999**, 20, 396–399.
- (8) Angers, S.; Salahpour, A.; Joly, E.; Hilairet, S.; Chelsky, D.; Dennis, M.; Bouvier, M. Detection of β 2-adrenergic receptor

- dimerization in living cells using bioluminescence resonance energy transfer (BRET). Proc. Natl. Acad. Sci. U. S. A. 2000, 97, 3684–3689.
- (9) Rocheville, M.; Lange, D. C.; Kumar, U.; Patel, S. C.; Patel, R. C.; Patel, Y. C. Receptors for dopamine and somatostatin: formation of hetero-oligomers with enhanced functional activity. *Science* **2000**, 288. 154–157.
- (10) Rodríguez-Frade, J. M.; Vila-Coro, A. J.; de Ana, A. M.; Albar, J. P.; Martínez, A. C.; Mellado, M. The chemokine monocyte chemoattractant protein-1 induces functional responses through dimerization of its receptor CCR2. *Proc. Natl. Acad. Sci. U. S. A.* 1999, 96, 3628–3633.
- (11) Terrillon, S.; Bouvier, M. Roles of G-protein-coupled receptor dimerization: From ontogeny to signalling regulation. *EMBO Rep.* **2004**, *5*, 30–34.
- (12) Marullo, S.; Bouvier, M. Resonance energy transfer approaches in molecular pharmacology and beyond. *Trends Pharmacol. Sci.* **2007**, 28, 362–365.
- (13) Harding, P. J.; Attrill, H.; Boehringer, J.; Ross, S.; Wadhams, G. H.; Smith, E.; Armitage, J. P.; Watts, A. Constitutive dimerization of the G-protein coupled receptor, neurotensin receptor 1, reconstituted into phospholipid bilayers. *Biophys. J.* **2009**, *96*, 964–973.
- (14) Paila, Y. D.; Chattopadhyay, A. The function of G-protein coupled receptors and membrane cholesterol: specific or general interaction? *Glycoconjugate J.* **2009**, *26*, 711–720.
- (15) Paila, Y. D.; Tiwari, S.; Chattopadhyay, A. Are specific nonannular cholesterol binding sites present in G-protein coupled receptors? *Biochim. Biophys. Acta, Biomembr.* **2009**, *1788*, 295–302.
- (16) Gimpl, G.; Wiegand, V.; Burger, K.; Fahrenholz, F. Cholesterol and steroid hormones: modulators of oxytocin receptor function. *Prog. Brain Res.* **2002**, *139*, 43–56.
- (17) Gimpl, G.; Burger, K.; Fahrenholz, F. A closer look at the cholesterol sensor. *Trends Biochem. Sci.* **2002**, *27*, 596–599.
- (18) Lee, A. G. How lipids affect the activities of integral membrane proteins. *Biochim. Biophys. Acta, Biomembr.* **2004**, *1666*, 62–87.
- (19) Ohvo-Rekilä, H.; Ramstedt, B.; Leppimäki, P.; Slotte, J. P. Cholesterol interactions with phospholipids in membranes. *Prog. Lipid Res.* **2002**, *41*, 66–97.
- (20) Béjà, O.; Aravind, L.; Koonin, E. V.; Suzuki, M. T.; Hadd, A.; Nguyen, L. P.; Jovanovich, S. B.; Gates, C. M.; Feldman, R. A.; Spudich, J. L.; Spudich, E. N.; DeLong, E. F. Bacterial Rhodopsin: Evidence for a New Type of Phototrophy in the Sea. *Science* **2000**, 289, 1902–1906.
- (21) Béjà, O.; Spudich, E. N.; Spudich, J. L.; Leclerc, M.; DeLong, E. F. Proteorhodopsin Phototrophy in the Ocean. *Nature* **2001**, *411*, 786–789.
- (22) de la Torre, J. R.; Christianson, L. M.; Béjà, O.; Suzuki, M. T.; Karl, D. M.; Heidelberg, J.; DeLong, E. F. Proteorhodopsin genes are distributed among divergent marine bacterial taxa. *Proc. Natl. Acad. Sci. U. S. A.* **2003**, *100*, 12830–12835.
- (23) Gómez-Consarnau, L.; Needham, D. M.; Weber, P. K.; Fuhrman, J. A.; Mayali, X. Influence of Light on Particulate Organic Matter Utilization by Attached and Free-Living Marine Bacteria. *Frontiers in Microbiology* **2019**, *10*, DOI: 10.3389/fmicb.2019.01204.
- (24) Koedooder, C.; Van Geersdaële, R.; Guéneuguès, A.; Bouget, F.-Y.; Obernosterer, I.; Blain, S. The Interplay between Iron Limitation, Light, and Carbon in the Proteorhodopsin Containing Photobacterium Angustum S14. FEMS Microbiol. Ecol. 2020, DOI: 10.1093/femsec/fiaa103.
- (25) Marchetti, A.; Catlett, D.; Hopkinson, B. M.; Ellis, K.; Cassar, N. Marine Diatom Proteorhodopsins and Their Potential Role in Coping with Low Iron Availability. *ISME J.* **2015**, *9*, 2745–2748.
- (26) Klyszejko, A. L.; Shastri, S.; Mari, S. A.; Grubmüller, H.; Muller, D. J.; Glaubitz, C. Folding and Assembly of Proteorhodopsin. *J. Mol. Biol.* **2008**, 376, 35–41.
- (27) Maciejko, J.; Mehler, M.; Kaur, J.; Lieblein, T.; Morgner, N.; Ouari, O.; Tordo, P.; Becker-Baldus, J.; Glaubitz, C. Visualizing specific cross-protomer interactions in the homo-oligomeric membrane protein proteorhodopsin by dynamic-nuclear-polarization-enhanced solid-state NMR. J. Am. Chem. Soc. 2015, 137, 9032–9043.

- (28) Hussain, S.; Kinnebrew, M.; Schonenbach, N. S.; Aye, E.; Han, S. Functional consequences of the oligomeric assembly of proteorhodopsin. *J. Mol. Biol.* **2015**, 427, 1278–1290.
- (29) Han, C.-T.; Song, J.; Chan, T.; Pruett, C.; Han, S. Electrostatic Environment of Proteorhodopsin Affects the pKa of Its Buried Primary Proton Acceptor. *Biophys. J.* **2020**, *118*, 1838–1849.
- (30) Ran, T.; Ozorowski, G.; Gao, Y.; Sineshchekov, O.; Wang, W.; Spudich, J.; Luecke, H. Cross-protomer interaction with the photoactive site in oligomeric proteorhodopsin complexes. *Acta Crystallogr., Sect. D: Biol. Crystallogr.* **2013**, *69*, 1965–80.
- (31) Barrantes, F. J.; Fantini, J. From hopanoids to cholesterol: Molecular clocks of pentameric ligand-gated ion channels. *Prog. Lipid Res.* **2016**, *63*, 1–13.
- (32) Ourisson, G.; Albrecht, P. Hopanoids. 1. Geohopanoids: the most abundant natural products on Earth? *Acc. Chem. Res.* **1992**, 25, 398–402.
- (33) Pearson, A.; Flood Page, S. R.; Jorgenson, T. L.; Fischer, W. W.; Higgins, M. B. Novel hopanoid cyclases from the environment. *Environ. Microbiol.* **2007**, *9* (9), 2175–2188.
- (34) Wu, C.-H.; Bialecka-Fornal, M.; Newman, D. K. Methylation at the C-2 position of hopanoids increases rigidity in native bacterial membranes. *eLife* **2015**, *4*, e05663.
- (35) Tahara, Y.; Yuhara, H.; Yamada, Y. Distribution of Tetrahydroxy-bacteriohopane in the Membrane Fractions of Zymomonas mobilis. *Agric. Biol. Chem.* **1988**, *52*, 607–609.
- (36) Jürgens, U. J.; Simonin, P.; Rohmer, M. Localization and distribution of hopanoids in membrane systems of the cyanobacterium Synechocystis PCC 6714. FEMS Microbiol. Lett. 1992, 92, 285–288
- (37) Simonin, P.; Jürgens, U. J.; Rohmer, M. Bacterial Triterpenoids of the Hopane Series from the Prochlorophyte Prochlorothrix Hollandica and their Intracellular Localization. *Eur. J. Biochem.* **1996**, 241, 865–871.
- (38) Poralla, K.; Härtner, T.; Kannenberg, E. Effect of temperature and pH on the hopanoid content of Bacillus acidocaldarius. *FEMS Microbiol. Lett.* **1984**, 23, 253–256.
- (39) Poralla, K.; Kannenberg, E.; Blume, A. A glycolipid containing hopane isolated from the acidophilic, thermophilic bacillus acidocaldarius, has a cholesterol-like function in membranes. *FEBS Lett.* **1980**, *113*, 107–110.
- (40) Kannenberg, E.; Blume, A.; McElhaney, R. N.; Poralla, K. Monolayer and calorimetric studies of phosphatidylcholines containing branched-chain fatty acids and of their interactions with cholesterol and with a bacterial hopanoid in model membranes. *Biochim. Biophys. Acta, Biomembr.* 1983, 733, 111–116.
- (41) Nagumo, A.; Sato, Y.; Suzuki, Y. Electron Spin Resonance Studies of Phosphatidylcholine Interacted with Cholesterol and with a Hopanoid in Liposomal Membrane. *Chem. Pharm. Bull.* **1991**, 39, 3071–3074.
- (42) Sáenz, J. P.; Sezgin, E.; Schwille, P.; Simons, K. Functional convergence of hopanoids and sterols in membrane ordering. *Proc. Natl. Acad. Sci. U. S. A.* **2012**, *109*, 14236–14240.
- (43) Sáenz, J. P.; Grosser, D.; Bradley, A. S.; Lagny, T. J.; Lavrynenko, O.; Broda, M.; Simons, K. Hopanoids as functional analogues of cholesterol in bacterial membranes. *Proc. Natl. Acad. Sci. U. S. A.* **2015**, *112*, 11971–11976.
- (44) Sáenz, J. P. Hopanoid enrichment in a detergent resistant membrane fraction of Crocosphaera watsonii: Implications for bacterial lipid raft formation. *Org. Geochem.* **2010**, *41*, 853–856.
- (45) Brown, D.; London, E. Structure and function of sphingolipidand cholesterol-rich membrane rafts. *J. Biol. Chem.* **2000**, 275, 17221–17224
- (46) Lingwood, D.; Simons, K. Lipid Rafts As a Membrane-Organizing Principle. *Science* **2010**, 327, 46–50.
- (47) Simons, K.; Ikonen, E. Functional rafts in cell membranes. *Nature* 1997, 387, 569–572.
- (48) Lingwood, D.; Kaiser, H.-J.; Levental, I.; Simons, K. Lipid rafts as functional heterogeneity in cell membranes. *Biochem. Soc. Trans.* **2009**, *37*, 955–960.

- (49) Lee, J. Y.; Lyman, E. Predictions for Cholesterol Interaction Sites on the A2A Adenosine Receptor. *J. Am. Chem. Soc.* **2012**, *134*, 16512–16515. PMID: 23005256.
- (50) Song, W.; Duncan, A. L.; Sansom, M. S. P. GPCR Oligomerisation Modulation by Conformational State and Lipid Interactions Revealed by MD Simulations and Markov Models. bioRxiv 2020, DOI: 10.1101/2020.06.24.168260.
- (51) Song, W.; Yen, H.-Y.; Robinson, C. V.; Sansom, M. S. P. State-Dependent Lipid Interactions with the A2a Receptor Revealed by MD Simulations Using In Vivo-Mimetic Membranes. *Structure* **2019**, 27, 392.
- (52) Arnarez, C.; Marrink, S. J.; Periole, X. Molecular Mechanism of Cardiolipin-Mediated Assembly of Respiratory Chain Supercomplexes. *Chemical Science* **2016**, *7*, 4435–4443.
- (53) Provasi, D.; Boz, M. B.; Johnston, J. M.; Filizola, M. Preferred Supramolecular Organization and Dimer Interfaces of Opioid Receptors from Simulated Self-Association. *PLoS Comput. Biol.* **2015**, *11*, e1004148.
- (54) Rassam, P.; et al. Supramolecular Assemblies Underpin Turnover of Outer Membrane Proteins in Bacteria. *Nature* **2015**, 523, 333–336.
- (55) Poger, D.; Mark, A. E. The Relative Effect of Sterols and Hopanoids on Lipid Bilayers: When Comparable Is Not Identical. *J. Phys. Chem. B* **2013**, *117*, 16129–16140.
- (56) Melo, M. N.; Ingólfsson, H. I.; Marrink, S. J. Parameters for Martini sterols and hopanoids based on a virtual-site description. *J. Chem. Phys.* **2015**, *143*, 243152.
- (57) Brooks, B. R.; et al. CHARMM: The biomolecular simulation program. *J. Comput. Chem.* **2009**, *30*, 1545–1614.
- (58) de Jong, D. H.; Singh, G.; Bennett, W. F. D.; Arnarez, C.; Wassenaar, T. A.; Schäfer, L. V.; Periole, X.; Tieleman, D. P.; Marrink, S. J. Improved Parameters for the Martini Coarse-Grained Protein Force Field. *J. Chem. Theory Comput.* **2013**, *9*, 687–697. PMID: 26589065.
- (59) Periole, X.; Cavalli, M.; Marrink, S.-J.; Ceruso, M. A. Combining an Elastic Network With a Coarse-Grained Molecular Force Field: Structure, Dynamics, and Intermolecular Recognition. *J. Chem. Theory Comput.* **2009**, *5*, 2531–2543. PMID: 26616630.
- (60) Wassenaar, T. A.; Ingólfsson, H. I.; Böckmann, R. A.; Tieleman, D. P.; Marrink, S. J. Computational Lipidomics with insane: A Versatile Tool for Generating Custom Membranes for Molecular Simulations. J. Chem. Theory Comput. 2015, 11, 2144–2155. PMID: 26574417.
- (61) Yesylevskyy, S. O.; Schäfer, L. V.; Sengupta, D.; Marrink, S. J. Polarizable Water Model for the Coarse-Grained MARTINI Force Field. *PLOS Computational Biology* **2010**, *6*, 1–17.
- (62) Marrink, S. J.; Risselada, H. J.; Yefimov, S.; Tieleman, D. P.; de Vries, A. H. The MARTINI Force Field:? Coarse Grained Model for Biomolecular Simulations. *J. Phys. Chem. B* **2007**, *111*, 7812–7824. PMID: 17569554.
- (63) Bussi, G.; Donadio, D.; Parrinello, M. Canonical sampling through velocity rescaling. *J. Chem. Phys.* **2007**, *126*, 014101.
- (64) Martoňák, R.; Laio, A.; Parrinello, M. Predicting crystal structures: the Parrinello-Rahman method revisited. *Phys. Rev. Lett.* **2003**, *90*, 075503.
- (65) Abraham, M. J.; Murtola, T.; Schulz, R.; Páll, S.; Smith, J. C.; Hess, B.; Lindahl, E. GROMACS: High performance molecular simulations through multi-level parallelism from laptops to supercomputers. *SoftwareX* **2015**, *1*–2, 19–25.
- (66) Lyman, E.; Zuckerman, D. M. On the structural convergence of biomolecular simulations by determination of the effective sample size. *J. Phys. Chem. B* **2007**, *111*, 12876–12882.
- (67) Trott, O.; Olson, A. J. AutoDock Vina: Improving the Speed and Accuracy of Docking with a New Scoring Function, Efficient Optimization, and Multithreading. *J. Comput. Chem.* **2010**, 31, 455–461.
- (68) Morris, G. M.; Huey, R.; Lindstrom, W.; Sanner, M. F.; Belew, R. K.; Goodsell, D. S.; Olson, A. J. AutoDock4 and AutoDockTools4:

- Automated Docking with Selective Receptor Flexibility. J. Comput. Chem. 2009, 30, 2785–2791.
- (69) Buchoux, S. FATSLiM: a fast and robust software to analyze MD simulations of membranes. *Bioinformatics* **2017**, *33*, 133–134.
- (70) Romo, T. D.; Leioatts, N.; Grossfield, A. Lightweight object oriented structure analysis: Tools for building tools to analyze molecular dynamics simulations. *J. Comput. Chem.* **2014**, *35*, 2305–2318.
- (71) Daura, X.; Gademann, K.; Jaun, B.; Seebach, D.; van Gunsteren, W. F.; Mark, A. E. Peptide Folding: When Simulation Meets Experiment. *Angew. Chem., Int. Ed.* **1999**, *38*, 236–240.
- (72) Stockton, G. W.; Smith, I. C. P. A Deuterium Nuclear Magnetic Resonance Study of the Condensing Effect of Cholesterol on Egg Phosphatidylcholine Bilayer Membranes. I. Perdeuterated Fatty Acid Probes. *Chem. Phys. Lipids* **1976**, *17*, 251–263.
- (73) Leftin, A.; Molugu, T. R.; Job, C.; Beyer, K.; Brown, M. F. Area per Lipid and Cholesterol Interactions in Membranes from Separated Local-Field (13)c NMR Spectroscopy. *Biophys. J.* **2014**, *107*, 2274–2286.
- (74) Hénin, J.; Salari, R.; Murlidaran, S.; Brannigan, G. A Predicted Binding Site for Cholesterol on the GABAA Receptor. *Biophys. J.* **2014**, *106*, 1938–1949.
- (75) Brannigan, G.; Hénin, J.; Law, R.; Eckenhoff, R.; Klein, M. L. Embedded cholesterol in the nicotinic acetylcholine receptor. *Proc. Natl. Acad. Sci. U. S. A.* **2008**, *105*, 14418–14423.
- (76) Hanson, M. A.; Cherezov, V.; Griffith, M. T.; Roth, C. B.; Jaakola, V.-P.; Chien, E. Y.; Velasquez, J.; Kuhn, P.; Stevens, R. C. A specific cholesterol binding site is established by the 2.8 Å structure of the human β 2-adrenergic receptor. *Structure* **2008**, *16*, 897–905.
- (77) Li, H.; Papadopoulos, V. Peripheral-type benzodiazepine receptor function in cholesterol transport. Identification of a putative cholesterol recognition/interaction amino acid sequence and consensus pattern. *Endocrinology* **1998**, *139*, 4991–4997.
- (78) Baier, C. J.; Fantini, J.; Barrantes, F. J. Disclosure of cholesterol recognition motifs in transmembrane domains of the human nicotinic acetylcholine receptor. *Sci. Rep.* **2011**, *1*, 69.
- (79) Gimpl, G. Interaction of G Protein Coupled Receptors and Cholesterol. *Chem. Phys. Lipids* **2016**, 199, 61–73.
- (80) Stone, K. M.; Voska, J.; Kinnebrew, M.; Pavlova, A.; Junk, M. J.; Han, S. Structural insight into proteorhodopsin oligomers. *Biophys. J.* **2013**, *104*, 472–481.
- (81) Liang, H.; Whited, G.; Nguyen, C.; Stucky, G. D. The directed cooperative assembly of proteorhodopsin into 2D and 3D polarized arrays. *Proc. Natl. Acad. Sci. U. S. A.* **2007**, *104*, 8212–8217.
- (82) Idso, M. N.; Baxter, N. R.; Narayanan, S.; Chang, E.; Fisher, J.; Chmelka, B. F.; Han, S. Proteorhodopsin function is primarily mediated by oligomerization in different micellar surfactant solutions. *J. Phys. Chem. B* **2019**, *123*, 4180–4192.
- (83) Luecke, H.; Schobert, B.; Richter, H.-T.; Cartailler, J.-P.; Lanyi, J. K. Structure of Bacteriorhodopsin at 1.55 Å Resolution. *J. Mol. Biol.* **1999**, 291, 899–911.
- (84) Kovalev, K.; Polovinkin, V.; Gushchin, I.; Alekseev, A.; Shevchenko, V.; Borshchevskiy, V.; Astashkin, R.; Balandin, T.; Bratanov, D.; Vaganova, S.; Popov, A.; Chupin, V.; Büldt, G.; Bamberg, E.; Gordeliy, V. Structure and Mechanisms of Sodium-Pumping KR2 Rhodopsin. *Science Advances* 2019, 5, eaav2671.
- (85) Morizumi, T.; Ou, W.-L.; Van Eps, N.; Inoue, K.; Kandori, H.; Brown, L. S.; Ernst, O. P. X-ray crystallographic Structure and oligomerization of Gloeobacter Rhodopsin. *Sci. Rep.* **2019**, *9*, 1–14.
- (86) Prasanna, X.; Mohole, M.; Chattopadhyay, A.; Sengupta, D. Role of Cholesterol-Mediated Effects in GPCR Heterodimers. *Chem. Phys. Lipids* **2020**, 227, 104852.
- (87) Alessandri, R.; Souza, P. C. T.; Thallmair, S.; Melo, M. N.; de Vries, A. H.; Marrink, S. J. Pitfalls of the Martini Model. *J. Chem. Theory Comput.* **2019**, *15*, 5448.
- (88) Jarin, Z.; Newhouse, J.; Voth, G. A. Coarse-Grained Force Fields from the Perspective of Statistical Mechanics: Better Understanding of the Origins of a MARTINI Hangover. *J. Chem. Theory Comput.* **2021**, *17*, 1170–1180.

- (89) Corradi, V.; Mendez-Villuendas, E.; Ingólfsson, H. I.; Gu, R.-X.; Siuda, I.; Melo, M. N.; Moussatova, A.; DeGagné, L. J.; Sejdiu, B. I.; Singh, G.; Wassenaar, T. A.; Delgado Magnero, K.; Marrink, S. J.; Tieleman, D. P. Lipid–Protein Interactions Are Unique Fingerprints for Membrane Proteins. ACS Cent. Sci. 2018, 4, 709–717.
- (90) Duncan, A. L.; Corey, R. A.; Sansom, M. S. P. Defining How Multiple Lipid Species Interact with Inward Rectifier Potassium (Kir2) Channels. *Proc. Natl. Acad. Sci. U. S. A.* **2020**, *117*, 7803–7813.